Received: 12 October 2023 | Revised: 4 March 2024 | Accepted: 8 March 2024

DOI: 10.1111/pce.14891

ORIGINAL ARTICLE

Plant, Cell & Environment | WILEY

Incorporating photosynthetic acclimation improves stomatal optimisation models

Victor Flo[1,2] | Jaideep Joshi[3,4,5,6] | Manon Sabot[7,8,9] | David Sandoval[1] | Iain Colin Prentice[1]

[1]Department of Life Sciences, Georgina Mace Centre for the Living Planet, Imperial College London, Silwood Park Campus, Ascot, UK

[2]Departament de Biologia Animal, Biologia Vegetal i Ecologia, Univ Autònoma de Barcelona, Cerdanyola del Vallès, Spain

[3]Department of Geosciences, Institute of Geography, University of Bern, Bern, Switzerland

[4]Oeschger Centre for Climate Change Research, Faculty of Science, University of Bern, Bern, Switzerland

[5]Advancing Systems Analysis Program, International Institute for Applied Systems Analysis, Laxenburg, Austria

[6]Complexity Science and Evolution Unit, Okinawa Institute of Science and Technology Graduate University, Onna, Okinawa, Japan

[7]ARC Centre of Excellence for Climate Extremes, Sydney, New South Wales, Australia

[8]Climate Change Research Centre, University of New South Wales, Sydney, New South Wales, Australia

[9]Department of Biogeochemical Signals, Max Planck Institute for Biogeochemistry, Jena, Germany

Correspondence

Victor Flo, Department of Life Sciences, Georgina Mace Centre for the Living Planet, Imperial College London, Silwood Park Campus, Ascot SL5 7PY, UK.
Email: vflosierra@gmail.com

Funding information

H2020 European Research Council; Schmidt Futures programme; National Member Organizations; Strategic Initiatives Program of the International Institute for Applied Systems Analysis; H2020 Marie Sklodowska-Curie Actions; Australian Research Council; MICIU/AEI/10.13039/501100011033; NextGenerationEU/PRTR

Abstract

Stomatal opening in plant leaves is regulated through a balance of carbon and water exchange under different environmental conditions. Accurate estimation of stomatal regulation is crucial for understanding how plants respond to changing environmental conditions, particularly under climate change. A new generation of optimality-based modelling schemes determines instantaneous stomatal responses from a balance of trade-offs between carbon gains and hydraulic costs, but most such schemes do not account for biochemical acclimation in response to drought. Here, we compare the performance of six instantaneous stomatal optimisation models with and without accounting for photosynthetic acclimation. Using experimental data from 37 plant species, we found that accounting for photosynthetic acclimation improves the prediction of carbon assimilation in a majority of the tested models. Photosynthetic acclimation contributed significantly to the reduction of photosynthesis under drought conditions in all tested models. Drought effects on photosynthesis could not accurately be explained by the hydraulic impairment functions embedded in the stomatal models alone, indicating that photosynthetic acclimation must be considered to improve estimates of carbon assimilation during drought.

KEYWORDS

carbon assimilation, photosynthetic cost, soil drought, stomatal conductance, stomatal limitation

1 | INTRODUCTION

Accurate estimation of net photosynthetic rates (A_{net}) in terrestrial ecosystems is crucial for understanding and predicting vegetation dynamics, global carbon budgets, and climate change trends (Arora et al., 2020; Fisher & Koven, 2020; Green et al., 2019; Humphrey et al., 2021; Lombardozzi et al., 2015; Mercado et al., 2018). However, photosynthesis modules within current Ecosystem and Earth System models often lack accuracy and provide biased estimates of carbon assimilation (Prentice et al., 2015; Rogers et al., 2017; Seiler et al., 2022). This is explained, among other factors, by the inability of large-scale models to adequately account for the effects of drought on the regulation of stomatal gas exchange and leaf photosynthetic capacity (Zhou et al., 2013). Novel hydraulically explicit stomatal optimisation models that mechanistically incorporate drought impacts have shown promise in improving the accuracy of instantaneous gas exchange predictions, and therefore A_{net}, in terrestrial models (Eller et al., 2020; Sabot et al., 2020; Wang & Frankenberg, 2022a), while reducing their reliance on poorly constrained empirical parameters. Previous studies have thoroughly evaluated the performance of a variety of such models (Sabot et al., 2022b; Wang et al., 2020), and have advocated the testing of mid-term and transient non-stomatal constrains alongside stomatal limitations to photosynthesis: particularly the acclimation of photosynthetic capacity to drought.

Drought is a major abiotic stressor that affects plant growth and productivity (Ahlström et al., 2015; Kannenberg et al., 2020; Ruehr et al., 2019; Stocker et al., 2019). Under soil drought conditions and/or significantly increased atmospheric vapour pressure deficit (VPD), plants typically decrease their stomatal conductance (g_s), thus reducing water use and protecting their hydraulic system from embolism. However, a decrease in g_s leads to a reduction in CO_2 diffusion into the leaves, which in turn results in a decrease in A_{net}. Therefore, regulating g_s entails a trade-off between uptake of CO_2 for photosynthesis and managing hydraulic risks. As A_{net} declines during drought, maximum leaf photosynthetic capacity also declines associated with reduced a ribulose-1,5-bisphosphate (RuBP) turnover and ATP synthesis (Flexas & Medrano, 2002; Martin-StPaul et al., 2012; Peguero-Pina et al., 2009; Salmon et al., 2020; Zhou et al., 2013). Downregulation of photosynthetic capacity has also been proposed to be associated with photochemical inhibition by elevated sugar concentrations in mesophyll cells (Hölttä et al., 2017; Salmon et al.,2020), as well as increased abscisic acid accumulation and electrolyte concentrations, inhibiting stromal enzymes (Kaiser, 1987). Although the specific proximate mechanisms governing drought-driven photosynthetic downregulation are not fully understood, it is plausible that its ultimate cause is the cost associated with maintaining photosynthetic capacity. Therefore, exploring its implications for stomatal control should provide a basis for improving the accuracy of photosynthetic predictions (Sabot et al., 2022b; Smith et al., 2019; Yang et al., 2019).

Stomatal optimisation models rest on the trade-off between the carbon gained by photosynthesis and the risks associated with water lost to transpiration (Cowan & Farquhar, 1977). Inspired by economic thinking, such trade-off optimisation is typically expressed in terms of a carbon profit equation (i.e., carbon gain minus carbon cost), where water loss is substituted for an equivalent carbon-based 'penalty' cost (Wang et al., 2020; Wolf et al., 2016). Thus, plants may take the opportunity for higher carbon gain by allowing more transpiration when water is cheap to use and forego carbon gain when it is costly. A major appeal of optimality-based stomatal models is that, unlike their empirical counterparts (e.g., Ball et al., 1987; Leuning, 1990, 1995), they avoid prescribing the sensitivities of g_s to the environment and, instead, let them emerge from the optimality criterion. The added value in using optimisation models is robustness, i.e., the ability to predict stomatal behaviour under new environmental conditions outside of those used for model parameterisation. A challenge, however, is in formulating the optimality criterion and transforming water loss into a penalty cost, owing to the variety of ways in which transpiration (and the ensuing soil water depletion) can impede physiological function (Wang et al., 2020). Following Cowan and Farquhar (1977), stomatal optimisation models originally considered a parametric marginal carbon cost of water use (Katul et al., 2009; Konrad et al., 2008; Manzoni et al., 2011; Medlyn et al., 2011). Yet it was never specified how these costs should vary with the environment, time, and species (Mäkelä, 1996; Manzoni et al., 2011, 2013; Schymanski et al., 2007; Wong et al., 1985). To address this issue, subsequent stomatal optimisation models have conceptualised the cost of water use as an impairment to hydraulic function arising from the cavitation of xylem vascular tissues (Anderegg et al., 2018; Buckley et al., 2023; Eller et al., 2020; Joshi et al., 2022; Lu et al., 2020; Sperry et al., 2017; Wang et al., 2020; Wolf et al., 2016). Note, however, that this solution does not resolve all dynamic gas exchange regulation uncertainties (Buckley et al., 2023).

Motivated by calls to include non-stomatal limitations in terrestrial models (Sun et al., 2014; Zhou et al., 2013)—constrains on photosynthesis arising from changes in photosynthetic capacity or mesophyll conductance, independent of stomatal function—some studies have attempted to account for non-stomatal limitations within stomatal optimisation criteria (Dewar et al., 2018; Dewar et al., 2021; Friend, 1991; Hölttä et al., 2017; Nadal-Sala et al., 2021; Novick et al., 2016; Yang et al., 2019). For instance, some of these studies attempted to capture gas exchange responses to variation in soil water availability, by maximising photosynthesis under a prescribed linear reduction in instantaneous photosynthetic capacity or mesophyll conductance with decreasing xylem pressure (Dewar et al., 2018) or increasing sucrose concentrations (Hölttä et al., 2017). However, while downregulation certainly occurs, this assumption of linear reduction is supported by little evidence (Wang et al., 2020). Other studies (Drake, 2017; Egea et al., 2011; Keenan et al., 2009; Knauer et al., 2019; Yang et al., 2019; Zhou et al., 2013, 2014) have relied on calibrated functions for prescribing the reduction in maximum photosynthetic capacity or of the maximum mesophyll conductance. Contrasting with the aforementioned approaches and building upon earlier work by Wolf et al. (2016) and the

photosynthetic coordination hypothesis (Smith & Keenan, 2020; Smith et al., 2019; Wang et al., 2017), Joshi et al. (2022) suggested adding metabolic impairment to hydraulic impairment within the stomatal optimisation procedure, by accounting for a marginal maintenance cost of photosynthetic capacity (α). How α changes across space and through time (e.g., with environmental growing conditions, with changes in other functional traits) is unclear, but metabolic impairments are usually correctly represented in models when they are allowed to vary over timescales of a few days (Caldararu et al., 2020; Haverd et al., 2018; Jiang et al., 2020; Sabot et al., 2022a), whereas stomatal regulation is presumed instantaneous (but see Buckley et al., 2023; Feng et al., 2022).

In this study, we investigated the effects of including an optimality-based representation of photosynthetic acclimation within six existing models. To that end, we extended their optimality criteria to consider a marginal maintenance cost of photosynthetic capacity α, as proposed in Joshi et al. (2022). We tested the performance of these modified models against observational data stemming from dry-down experiments on >35 C_3 species. Our main objective was to assess the ability of the extended models to predict A_{net} and g_s, compared to the original formulations (Objective 1). We also analysed the extent to which each model's estimates of A_{net} and g_s could be explained by hydraulic impairment versus photosynthetic acclimation limitation (Objective 2). Finally, we explored the relationship between the cost parameter α, hydraulic parameters, (sub)species-specific functional traits, and their environmental growth conditions (Objective 3). We expected that accounting for photosynthetic acclimation will improve A_{net} estimates for all models. Based on previous findings by Wang et al. (2020) and Sabot et al. (2022b), we also expected that, during soil dry-downs, hydraulic impairment would affect assimilation to a greater extent than the acclimation of photosynthetic capacity, albeit to varying degrees among models. Finally, we hypothesised that species characterised by high hydraulic vulnerability (less-negative *P50*) or high specific leaf area would have higher photosynthetic maintenance costs, and that "fast-growing but drought-sensitive" species would also have higher metabolic sensitivity to drought.

2 | METHODS

2.1 | Stomatal optimisation models

Hydraulics-enabled stomatal optimisation models couple water transport and carbon uptake through g_s (see Notes 1 in the Supporting Information Material). In these steady-state models, g_s links to leaf water potential (ψ_l) through a mass-balance of water, i.e., root-to-leaf water supply equals transpiration demand (Equation S5), whilst controlling the rate at which CO_2 diffuses within the leaf, and thus, A_{net} (Equation S6). A given model's optimality criterion works to adjust the instantaneous g_s (consequently, ψ_l) to maximise profit, i.e., A_{net} minus a carbon-equivalent hydraulic cost Θ (Equation 1). Stomatal optimisation models can be algebraically rearranged such that they differ only in the mathematical form of the Θ function (see Sabot et al., 2022b and Wang et al., 2020 for comprehensive reviews):

$$\max_{\psi_l<0}\left(A_{net}(\psi_l) - \Theta(\psi_l)\right). \tag{1}$$

Adopting the nomenclature used by Sabot et al. (2022b), the stomatal optimisation models considered here are: PMAX (Sperry et al., 2017), PMAX2 (Wang et al., 2020), SOX (Eller et al., 2018), SOX2 (Buckley et al., 2023), CGAIN (Lu et al., 2020), and PHYDRO (Joshi et al., 2022).

The PMAX model was proposed by Sperry et al. (2017) to express the stomatal cost of water loss based on plant hydraulic theory at a minimal parameter expense. The PMAX model balances a carbon gain function, where A_{net} is normalised by its maximum potential value (A_{max}) specific to the instantaneous environmental conditions, with a hydraulic risk function, also normalised, varying with ψ_l and soil water potential (ψ_s). A unique pairing of g_s and ψ_l hence maximises the difference between the normalised assimilation and risk functions. This model can also be expressed as in Equation (1) by multiplying both the gain function and hydraulic risk function by A_{max}, in which case Θ becomes

$$\Theta = A_{\max}\frac{k_{\psi_s} - k_{\psi_l}}{k_{\psi_s} - k_{\psi_{crit}}}, \tag{2}$$

where $k\psi$ is the hydraulic conductance at a given water potential (ψ) calculated using Eq. S3 (Notes 1 in Supporting Information Material), with the double-subscripts *s*, *l*, and *crit* representing soil, leaf, and critical water potentials, respectively. The hydraulic conductance at the critical water potential ($k\psi_{crit}$) represents the point at which the plant pays the maximum cost of canopy desiccation (Sperry et al., 2017). Here, $k\psi_{crit}$ is assumed to be zero for simplicity and generalisation across species (Venturas et al., 2018). Since we are assuming a xylem without height change or vulnerability curve segmentation, k_ψ can be used to proxy canopy conductance. This assumption might impact the sensitivity of stomatal responses to soil drought compared with reality where different hydraulic segments are not characterised by the same vulnerability curve (Wang & Frankenberg, 2022b). However, this simplification is a practical necessity due to the general lack of detailed data on segment-specific maximum hydraulic conductance and vulnerability curves.

The PMAX2 model was developed by Wang et al. (2020) to meet a specific set of mathematical and biological criteria for a biologically sensible Θ. The hydraulic impairment function of this model is based on penalising the instantaneous transpiration ($E(\psi_l)$) by its proximity to E_{crit}, i.e., $E(\psi_l)$ at the critical leaf water potential at which we assume hydraulic conductance is null ($\psi_l \rightarrow -\infty$). $E(\psi_l)$ is weighted by A_{net} in proportion to E_{crit} such that

$$\Theta = A_{net}\frac{E(\psi_l)}{E_{crit}} = A_{net}\frac{\int_{\psi_s}^{\psi_l} P(\psi)d\psi}{\int_{\psi_s}^{-\infty} P(\psi)d\psi}. \tag{3}$$

Here, the hydraulic impairment function is equivalent to the ratio of two integrals of the hydraulic vulnerability curve function (P(ψ)). The integral in the numerator ranges from ψ_s to ψ_l, and the improper integral in the denominator ranges from ψ_s to minus infinity (at $k\psi_{crit}$). P(ψ) is calculated using Equation S4.

The CGAIN stomatal optimisation model (Lu et al., 2020) was motivated by the fact that gas exchange may be regulated differently depending on soil water dry-down length and dessication return time. The model assumes a carbon cost (ϖ; μmol m^{-2} s^{-1}) to offset carbon gain, with the former representing an investment into recovering the hydraulic conductance lost to embolized xylem (Sabot et al., 2022b). While the original CGAIN model is solved over long time periods and can consider delayed effects of xylem recovery, as in Sabot et al. (2022b), we assume an instantaneous version with no lagged costs of xylem recovery. However, applying Lu et al.'s (2020) model instantaneously may be unfair because of the necessary simplifications. This simplified version of CGAIN is expressed as

$$\Theta = \varpi\left(\frac{K_{\max} - k_{\psi_l}}{K_{\max}}\right) = \varpi(1 - P(\psi_l)), \tag{4}$$

where K_{max} is the maximum whole-plant hydraulic conductance between the roots to the leaves.

The PHYDRO model (Joshi et al., 2022) took a phenomenological approach that relies on an impairment function proportional to the square of the differential between the soil and leaf water potential ($\Delta\psi 2$)

$$\Theta = \gamma\Delta\psi^2, \tag{5}$$

where γ (μmol m^{-2} s^{-1} MPa^{-2}) is a calibrated empirical parameter which determines species-specific hydraulic sensitivity. This model requires the use of a vulnerability curve that accounts for the outside-xylem hydraulic pathways in fine roots and leaves (see the 'Parameter calibrations and simulation experiments' section).

The SOX stomatal model (Eller et al., 2018) drew on the PMAX model but opted to directly impair A_{net} by the ratio of the hydraulic vulnerability curve evaluated at ψ_l to that of the vulnerability curve evaluated at ψ_s

$$\Theta = A_{net}\left(1 - \frac{P(\psi_l)}{P(\psi_s)}\right). \tag{6}$$

Finally, the SOX2 model proposed by Buckley et al. (2023) reworked the SOX model to account for the leaf physiological kinetic factors that affect leaf water potential dynamics. In this model the parameter ψ_{50} (i.e., the water potential at a 50% loss of hydraulic conductance) is tuned by a species-specific stomatal behaviour parameter, δ (dimensionless). The parameter b (dimensionless) is the steepness of the vulnerability curve

$$\Theta = A_{net}\frac{|\psi_l|^b}{|\delta\psi_{50}|^b + |\psi_l|^b}. \tag{7}$$

2.2 | Acclimation of the photosynthetic capacity

To calculate A_{net}, maximum photosynthetic capacity must be known. Following the photosynthetic model of Farquhar et al. (1980), A_{net} is determined by the lesser of two biochemical assimilation rates (A_j and A_c) that are functions of the absorbed irradiance (I_{abs}), leaf intercellular CO_2 concentration (Ci) and temperature (Equations S7 and S8), minus a leaf day respiration rate. The two rates A_j and A_c depend on the maximum rate of electron transport (J_{max}) and maximum rate of carboxylation capacity (V_{cmax}), respectively, with both J_{max} and V_{cmax} differing in their sensitivities to temperature. The parameter values that set J_{max} and V_{cmax} are typically standardised to 25°C ($J_{max,25}$ and $V_{cmax,25}$; Equations S14 and S15) and taken to be species, ecosystem, or functional-type averages, without accounting for variation in their standardised magnitudes (i.e., the ratio of $J_{max,25}$ to $V_{cmax,25}$ is a fixed value). However, J_{max} and V_{cmax} co-vary across species and in the medium to long term, leading to a coordination among the two photosynthetic rates (Chen et al., 1993; Maire et al., 2012).

Assuming coordination, we can establish a single cost for photosynthetic capacity, based on only one of the two limiting biochemical photosynthetic rates. Specifically, we let both J_{max} and V_{cmax} acclimate by extending the stomatal optimisation criterion (Equation 1) to account for the cost of maintaining electron-transport capacity (Joshi et al., 2022):

$$\max_{\psi_l<0}(A(\psi_l, J_{\max}) - \Theta(\psi_l) - \alpha J_{\max,25}(\psi_l)), \tag{8}$$

where α is a marginal maintenance cost per unit of electron-transport capacity under standard conditions (i.e., 25°C), and $\alpha J_{max,25}$ represents the total carbon cost required to maintain photosynthetic capacity. Here, unlike in Joshi et al. (2022), we optimise $J_{max,25}$ instead of J_{max}, to limit the effects of temperature on α.

The optimisation problem presented in Equation (8) allows for the estimation of the values of ψ_l and $Jmax,25$ that maximise profit, similarly to how Equation (1) allows for the regulation of ψ_l and, subsequently, g_s (Equation S5) to maximise A_{net}. The optimisation of $J_{max,25}$ is instantaneous, but it uses the environmental conditions at the time when gas exchange measurements were performed, averaged over the previous 7 days to capture the weekly acclimation timescale. We obtain the corresponding coordinated $V_{cmax,25}$ via the photosynthetic coordination hypothesis (Equations S10–S13; Smith et al., 2019; Smith & Keenan, 2020; Wang et al., 2017). The optimised acclimated parameter values of $J_{max,25}$ and $V_{cmax,25}$ are then adjusted to the instantaneous temperature using an Arrhenius function (Equations S14 and S15), and fed back as fixed parameters into the biochemical photosynthetic model for the calculation of instantaneous g_s, ψ_s, and A_{net} via Equation (1).

In our approach, photosynthetic capacity is acclimated not only to the prevailing atmospheric conditions of the previous 7-day period, but also to ψ_s through the averaged hydraulic cost or impairment factor. However, as soil moisture conditions were not available for all 7-day periods in the datasets used, to calculate the 7-day average we assumed that ψ_s decreased linearly between the first and the last days of the experiment. We also assumed that the environmental conditions were constant until the start of the experiment.

2.3 | Experimental data

We used published data from a series of dry-down experiments to evaluate the performance of the six stomatal optimisation models with or without accounting for the photosynthetic acclimation. Some of these experimental data were originally compiled from the published literature by Zhou et al. (2013). We complemented them with others found through a similar literature search on Google Scholar—in September 2022, we used the keywords '"stomatal conductance" and "photosynthesis" and "soil water potential" and "dry-down" or "drought" or "experiment"', yielding 490 references. Data were subsequently requested from the authors, collected from open databases, or digitised from published figures using GetData Graph Digitiser version 2.26.0.20. The data were filtered to ensure that the experiments fulfilled the following criteria: (1) individuals of the species were subjected to a controlled drought, (2) the growth conditions were recorded during the study period (i.e., VPD or relative humidity, temperature and radiation), and (3) simultaneous measurements of g_s, A_{net}, and soil water potential or pre-dawn leaf water potential were made. For one of the experiments (Salmon et al., 2020), we also included the values of the controls where the individuals were not exposed to drought (i.e., the soil water potential was above −1 MPa) to expand data limitations at high soil-water potentials. After filtering, data from 12 studies remained, for a total of 37 species and sub-species representing diverse plant functional types (Table S1, Figures S1 and S2).

2.4 | Species-specific plant traits

The stomatal optimisation models studied rely on a two-parameter hydraulic vulnerability curve (Equation S4) to simulate water transport from roots to leaves. At the species-level, values of the water potential at 50% loss of hydraulic conductance (ψ_{50}) were obtained from hydraulic trait databases [preferably Martin-StPaul et al. (2017), otherwise Choat et al. (2012)]. The slopes of the vulnerability curve (b) were estimated by equating Equation S4 to a cumulative Weibull distribution representing plant vulnerability to cavitation (Sperry et al., 2017), which depends on both ψ_{50} and the water potential at 12% loss of hydraulic conductance (ψ_{12}) or at 88% loss of hydraulic conductance (ψ_{88}) (with ψ_{12} and ψ_{88} obtained from the aforementioned hydraulic databases). When species-level ψ_{50}, ψ_{12} or ψ_{88} were not available (21 out of 38 species, Table S1), we imputed the missing values using environmental, phylogenetic, and trait correlations and covariations, following the methodology developed by Sanchez-Martinez et al. (2023). These correlations and covariations derived from the entire Xylem Functional Traits Database (Choat et al., 2012) alongside environmental data (mean annual temperature and average annual precipitation) extracted from the CHELSA database (Karger et al., 2017).

Further, to analyse the potential coordination between α and other plant traits (objective 3), we collected species-specific traits related to water use strategies and plant form and function. These were the species' maximum height (H_{max}; m), specific leaf area (SLA; $cm^2\ g^{-1}$), Huber value (Hv; i.e., sapwood area per leaf area in $cm_{sw}^2\ m_{leaf}^{-2}$), and maximum leaf-area specific hydraulic conductivity (K_L; mol m_{xylem} $mleaf^{-2}\ s^{-1}\ MPa^{-1}$), all of which were retrieved from the Xylem Functional Traits Database (Choat et al., 2012). Missing species-specific trait values were obtained by imputation (as described above for ψ_{50}, ψ_{12} and ψ_{88}), following Sanchez-Martinez et al. (2023) (see Table S2 for the root mean square error [RMSE] of each imputed variable). In herbaceous species, hydraulic conductivities, ψ_{50}, ψ_{12} or ψ_{88} were interpreted at the whole-plant level.

2.5 | Parameter calibrations

Besides depending on estimates of of ψ_{50} and b for their parameterisation, all the stomatal optimisation models considered here rely on an estimate of K_{max} (mol $m^{-2}\ s^{-1}\ MPa^{-1}$; Equation S3) to set the maximum possible conductance to water flow between the roots and the leaves. Estimates of K_{max} available from the literature are seldom suitable for modelling efforts (because models require parametrisations of K_{max} at the scale of the whole plant, measured per unit leaf area; Mencuccini et al., 2019). Therefore, in this study, we have opted to calibrate the K_{max} of the PMAX, PMAX2, and SOX models for each species within each dry-down experiment. The SOX2, PHYDRO, and CGAIN models additionally rely on an estimate of a hydraulic cost parameter (δ, γ, and ϖ, respectively). Unless stated otherwise, we calibrated these models' hydraulic cost parameter but not their K_{max}, instead obtaining their K_{max} by calibrating the PMAX model which limits the potential for parameter un-determination.

Three different sets of parameter calibrations (Figure 1) were needed for us to address the objectives of this study. Although the number of calibration sets is a match for the study's objectives, note that Calibration 1 alone could not fully address Objective 1, nor could Calibration 2 alone address Objective 2.

Calibration 1 aimed to assess the models' performance without considering photosynthetic acclimation (i.e., α, $J_{max,25}$ and $V_{cmax,25}$ were not calibrated). To achieve this, we either calibrated K_{max} of PMAX, PMAX2, and SOX, or the hydraulic cost parameters of SOX2, PHYDRO, and CGAIN, based on the 80th wet percentile data of each species and dry-down experiment. This calibration procedure utilised a successive parabolic interpolation algorithm aiming to minimising the normalised root mean square error (NRMSE) between predicted and measured instantaneous rates of g_s, and A_{net},

$$NRMSE = \frac{\sum_{i=1}^{N}(g_s{}' - g_s)_i^2}{\left(\frac{\sum_{i=1}^{N} g_{s_i}}{N}\right)^2} + \frac{\sum_{i=1}^{N}(A_{net}{}' - A_{net})_i^2}{\left(\frac{\sum_{i=1}^{N} A_{net_i}}{N}\right)^2}, \quad (9)$$

where the double-subscript i represents the position of the paired predicted and actual values, and N is the total number of actual observations for a given species in an experiment.

Calibration 2 considered photosynthetic acclimation. In Calibration 2, we utilised the hydraulic parameter values obtained in Calibration 1 and calibrated α on the 80th wet percentile data of the

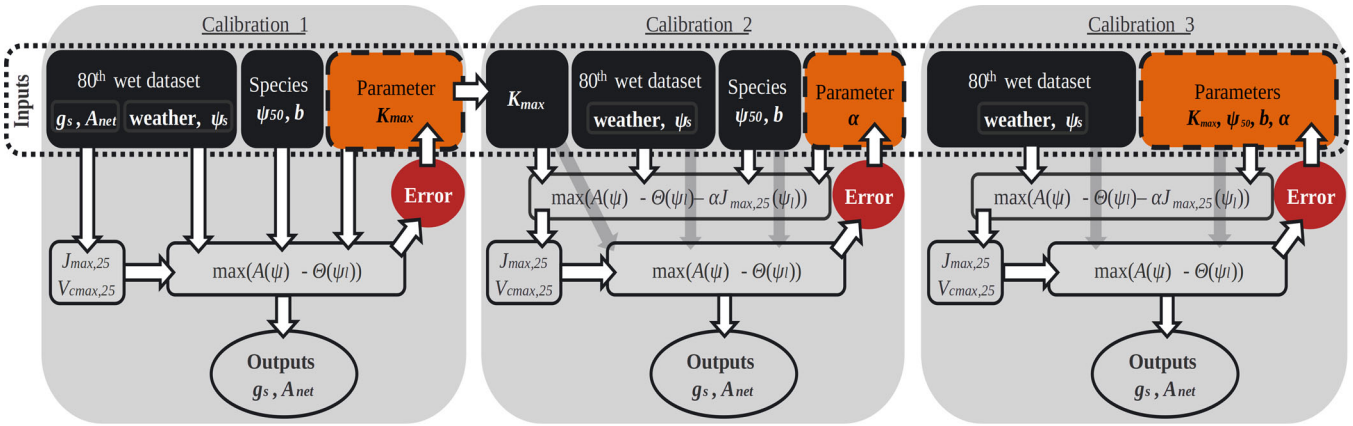

FIGURE 1 Schematics of the three sets of parameter calibrations performed for PMAX, PMAX2, and SOX models, i.e., models free of a hydraulic cost parameter. Calibration 1 focused on calibrating the K_{max} of each species-experiment and model. In Calibration 2, the α parameter of each species-experiment and model was calibrated, using the K_{max} parameter from Calibration 1. Calibration 3 involve calibrating the K_{max}, ψ_{50}, b, α parameters of each species-experiment and model. Parameter calibration was achieved by minimising the error between predicted and measured instantaneous g_s and A_{net}, using Equation (9). The dashed box illustrates the parameters estimated in each calibration set. Calibrations 2 and 3 included photosynthetic acclimation. Because they required a slightly different calibration procedure (see Parameter calibrations section), the models relying on a hydraulic cost parameter besides just K_{max} (SOX2, PHYDRO, CGAIN) are not included in the schematic. [Color figure can be viewed at wileyonlinelibrary.com]

species and dry-down experiment (specific α). The calibration process followed the same parameter optimisation algorithm as in Calibration 1. We accounted for photosynthetic acclimation as described in the 'Acclimation of the photosynthetic capacity' section (Equation 8).

Calibration 3 accounted for photosynthetic acclimation as Calibration 2 but, this time, more model parameters were calibrated. Using the Nelder-Mead algorithm, we looked to fit the best {K_{max}, ψ_{50}, b, α} parameter set for each individual model, species, and dry-down experiment that minimised Equation (9). In the case of the SOX2, PHYDRO, and CGAIN models, we also calibrated their respective hydraulic cost parameter (i.e., δ, γ and ϖ) in addition to the {K_{max}, ψ_{50}, b, α} parameter sets. Calibration 3 was performed on the entire dataset of each species-experiment, and it was also repeated without photosynthetic acclimation (i.e., α was not included; Equation 1). Calibrating four or five parameters on small data subsets (e.g., $N = 4$; Table S1) likely leads to unrealistic predictions of these parameters. Therefore, the parameter estimates from small data samples were given less weight in subsequent statistical analyses.

2.6 | Simulation experiments

The following simulation experiments were performed to address the study's objectives:

Objective 1: To compare the performance of the models with and without acclimation, we made three types of predictions for g_s and A_{net}. These predictions were "non-acclimated" (using the parameters from Calibration 1), "acclimated with specific α" (using the parameters from Calibration 2), and "acclimated with average α". We extracted the average α (0.0962) of all species from Calibration 3 by fitting a mixed-effects linear model with crossed random intercept for stomatal models, species, and dry-down experiments. Many data sources provided data for several species, whilst some comprised only one species, and the same species could also found across data sources. This unevenness of data motivated our choice of a simple crossed random structure that provides global, species population-average intercepts while accommodating both source and model variations. Note that both the non-acclimated (Equation 1) and acclimated (Equation 9) model simulations performed for Objective 1 spanned the entire dry-down for a given species-experiment and, as such, were mostly outside their calibration samples (restricted to the 80th wet percentile of data, see Parameter calibrations section). Finally, we opted to use the hydraulic (or hydraulic cost) parameters obtained for the non-acclimated models (Calibration 1) when running their acclimated counterparts (Calibration 2), thus reducing model-specific degrees of freedom, and making the simulation outcomes as comparable as possible across models.

Objective 2: To gain insight into the relative contributions of hydraulic (stomatal) versus photosynthetic acclimation limitations on photosynthesis, we used the "non-acclimated" and the "acclimated with specific α" simulations from Objective 1.

Objective 3: To explore the co-variation of α with hydraulic (or hydraulic cost) parameters in different models and in relation to other functional traits and environmental conditions, we used simulations of g_s and A_{net} generated by using the full model-specific parameter sets from Calibration 3 (i.e., obtained with and without acclimation).

2.7 | Additional parameter specifications and forcing data

In Calibrations 1 and 2, we used species-specific values of ψ_{50} and b retrieved from the literature (Table S1). However, for the PHYDRO

model, instead of using the parameters of the xylem vulnerability curve, we used an approximate estimate of the outside-xylem (ox) vulnerability curve by setting $\psi_{ox50} = \psi_{50}/3$ and $b = 1$, based on the findings of Joshi et al. (2022). To ensure that using a different parameterisation of hydraulic vulnerability did not give the PHYDRO model an unfair advantage or disadvantage compared to other models, we repeated the first and second set of calibrations (and associated simulations) using outside-xylem vulnerability curve parameters (i.e., $\psi_{ox50} = \psi_{50}/3$ and $b = 1$) for other models and xylem vulnerability curve parameters (i.e., ψ_{50} and b) for PHYDRO. This incidentally provided us with a test of the sensitivity of the models to the choice of vulnerability curve parameters.

In all calibrations and model simulations that did not account for acclimation (i.e., Calibration 1, Calibration 3 without acclimation, and "non-acclimated" simulations), $J_{max,25}$ and $V_{cmax,25}$ parameters were obtained from the average values of the actual g_s and A_{net} measurements for the 80th wet percentile of each species-study (Figures S1 and S2), and assuming photosynthetic coordination via Equations S6, S11, S12, and S13.

The model calibrations and simulations were driven by observed soil water potential, VPD, temperature, and radiation. When acclimation was not considered (Equation 1), we preferentially used instantaneous data. Instantaneous soil water potential was always available, however, in cases where instantaneous records of VPD, temperature, and radiation were not, we used the average values of the entire experimental period for VPD, temperature, and radiation. The latter option was also chosen when calibrating and simulating acclimation via Equation (8).

2.8 | Statistical analyses

The performance of the six stomatal models in predicting A_{net} with and without acclimation (Objective 1) was assessed using four statistical metrics. These metrics were applied at the species level, for each different stomatal models, and using three simulation scenarios—those without acclimation, with acclimation using average α, and with acclimation using specific α. The metrics include: (1) Pearson's correlation coefficient, where coefficients close to 1 indicate a perfect positive correlation between the estimated and actual A_{net}; values <0 indicate a negative correlation. (2) The slope (m) of a linear relationship between the estimated and actual A_{net}, which measures the proportional bias of a model's predictions. Values of m close to 1 indicate good proportionality between the estimated and actual A_{net}, whereas m much smaller/higher than 1 imply that the predicted A_{net} are underestimated/overestimated as the soils dry out. (3) The RMSE, measuring the cumulative absolute error of A_{net} predictions, with a larger penalty on larger errors. (4) The bias (Equation 10) of the A_{net} estimates, which evaluates the average simulation error and its direction. A negative bias implies that the estimated values are, on average, systematically higher than the actual values.

$$Bias = \frac{\sum_{i=1}^{N}(A_{net} - A_{net}')_i}{\sum_{i=1}^{N} A_{net_i}}. \quad (10)$$

For each statistical metric, we used linear mixed-effects models (LMMs) to further compare the performance of stomatal optimisation models. We explain the metric variance, using the stomatal model, the simulation scenario (i.e., "non-acclimated", "acclimated with average α", or "acclimated with specific α") and their interactions as fixed explanatory variables. The data source and species were used as crossed random intercepts to account for potential systematic errors in the experimental design or potential species-specific biases that could be introduced across stomatal stomatal models. All performance analyses were repeated for g_s.

We used models parametrised with (Calibration 2) or without acclimation (Calibration 1), to evaluate how each stomatal optimisation model divides its predictive capacity into the components of hydraulic impairment versus limitations due to photosynthetic acclimation (Objective 2). For each stomatal model, we analysed how the explained variability (R^2) of A_{net} was partitioned between the hydraulic penalty (stomatal partition), the cost of maintaining photosynthetic capacity ($\alpha J_{max,25}$; photosynthetic acclimation partition), and species. We accounted for the explained variability by species because species-level ψ_{50} and b parameters may be inadequate for a given population within the species. The variance explained by stomatal partition was calculated as the marginal R^2 of the actual A_{net} explained by the estimated A_{net} without acclimation, adjusting random intercepts for each species in an LMM. We then applied an LMM with the same structure, but using the estimated A_{net} values with acclimation as the explanatory variable instead. The variance explained by photosynthetic acclimation was determined by calculating the difference between the respective marginal R^2 of the latter and former statistical models. The species variance partition was obtained as the difference between the conditional and the marginal R^2 of the LMM for the acclimated A_{net} simulations. To understand whether the importance of these variance components changes as the soil dries, we repeated the analysis on the driest 50th percentile of data for each species within each dry-down experiment.

Finally, we analysed the relationships between the specific α from Calibration 3 and other species- and experiment-specific traits and growing conditions. The traits considered as possible explanatory variables for α were the species-level H_{max}, ψ_{50}, SLA, Hv, and K_L collected or imputed from the literature (Table S1). We selected these traits as they stand for different axes of variation representing different water use strategies and life forms. We also included an estimate of the actual $J_{max,25}$ under well-watered conditions (80th wet percentile; $J_{maxWW,25}$), which was inferred from the observed A_{net} and g_s using the one-point method (Equations S6, S11, S12, and S13; De Kauwe et al., 2016). The environmental conditions of interest were average I_{abs} and C_a during the experimental period. During the experiments, I_{abs} was strongly positively related to VPD and air temperature (Figure S3). All explanatory variables that presented a non-normal distribution (H_{max}, SLA, Hv, K_L, and $J_{maxWW,25}$) were transformed using the natural logarithm to minimise the leverage

effect of large values. We performed a multivariate LMM in which the variability of α was explained by the chosen species-level traits, ψ_{50}, J_{maxWW}, and the growing conditions, with the stomatal models and dry-down experiments used as crossed random intercepts. Because species-level traits were taken as fixed predictors of the LMM, it was important we used the stomatal models as random intercepts to account for the variability in α caused by each stomatal model for each species. Next, we identified the most significant predictors using an Akaike Information Criterion (AIC) stepwise algorithm. Finally, we calculated the variance inflation factor (VIF) of each predictor to explore possible multicollinearity across explanatory variables. We also repeated the above model and the identification of the most significant predictors using the product of α and $J_{maxWW,25}$, which corresponds to a photosynthetic capacity cost under well-watered conditions, as an explanatory variable.

In all LMMs, we used the natural logarithm of each species' sample size as a weighting factor to minimise the effect of a small number of data points (see N, Table S1).

2.9 | Code

All analyses and calibrations were performed using R 4.2.0 (R Core Team, 2022) and the code is freely available from GitHub at https://github.com/vflo/Acclimated_gs_optimization_models. The following specific R packages were used:

1. TrEvol (Sanchez-Martinez et al., 2023) for the imputation of missing species-level trait values (see the 'Species-specific model parametrisations and plant traits' section above);
2. dEoptim (Mullen et al., 2011) to solve the instantaneous optimality criteria presented in Equations (1) and (2), and (9) and (10);
3. lme4 (Bates et al., 2015) for all LMM computations (see 'Statistical analyses');
4. MuMIn (Bartoń, 2020) for the R^2 variance partitions ('Statistical analyses').

3 | RESULTS

All three calibration sets were successful for all the species and stomatal models. Most of the model parameterisations obtained from Calibration 3 were insensitive to acclimation (Figures S4a, S4b and S4c), with the exception of the magnitude of -ψ_{50} and K_{max} from SOX and SOX2 which were reduced by acclimation, and the parameter b in the PMAX model that was moderately reduced by acclimation ($p < 0.05$). In Calibration 1, where K_{max} was the only calibrated parameter for PMAX, PMAX2 and SOX, the K_{max} of these three models were much lower than those from Calibration 3 in the absence of acclimation (Figure S4a). For PMAX and PMAX2, K_{max} also substantially decreased between Calibration 3 accounting for acclimation and Calibration 1 (Figure S4a).

3.1 | Model performance with versus without photosynthetic acclimation

All six stomatal models generated highly and positively correlated in-sample A_{net} estimates across most species (Figure 2a, Figures S2 and S5). The mean Pearson's correlation coefficient for the stomatal models without acclimation ranged from 0.755 in PMAX2 to 0.810 in PHYDRO, whilst for the acclimated stomatal models using the average α, it ranged between 0.803 and 0.825 in SOX2 and PHYDRO, respectively, and using the specific α, it ranged from 0.794 in SOX to 0.817 in PMAX (Figure 2a). The incorporation of acclimation, using both the average and the specific α, produced a moderately positive effect on the estimates of PMAX2 in terms of correlation. In the case of PMAX, this positive effect was observed with the average α. However, for CGAIN, PHYDRO, SOX, and SOX2, the effect was negligible (Figure 2a).

By contrast, the slope between the predicted and actual A_{net} values (m) was strongly influenced by acclimation. Accounting for acclimation led to m values closer to 1. Conversely, without accounting for acclimation, m was significantly larger than 1 (Figure 2b), as the models were unable to accurately simulate the downregulation of A_{net} as the soil dried out in the absence of acclimation in some species (Figure S2). Upon acclimation, the average values of m for CGAIN, PHYDRO, PMAX, SOX, and SOX2 were not likely to differ from one ($H_1 \neq 1$; $p > 0.05$), indicating that these five models' estimates of A_{net} were in good proportionality to the observations as the soil dried. The average m of PMAX2 was greater than 1 though, most probably because it failed in a few species-experiments with a large N (Figure 2b).

The different models did not significantly differ from one another in their average non-acclimated RMSE. Acclimated models with species-experiment specific α (i.e., specific α acclimated from Calibration 2), all displayed a significantly lower RMSE than those without acclimation (Figure 2c). In addition, the average α acclimated SOX2 had significantly lower RMSE than without acclimation. The average α acclimated PHYDRO and CGAIN had significantly higher RMSE than PMAX and SOX, and in the case of CGAIN, higher than SOX2 as well (Table S3). The specific α acclimated PHYDRO presented the lowest average RMSE for A_{net} at 3.07 $\mu molc\ m^{-2}\ s^{-1}$ (Figure 2c, Table S3), whereas the average α acclimated CGAIN presented the highest average RMSE at 5.07 $\mu molc\ m^{-2}\ s^{-1}$.

All the specific α acclimated models presented biases significantly lower than the non-acclimated models and not significantly different to zero. PHYDRO, CGAIN, PMAX and PMAX2 did not show significant differences in biases between their average α acclimated and their non-acclimated model versions (Figure 2d). All the non-acclimated stomatal models presented a significant average overestimation (bias higher than zero; $p < 0.05$), with PMAX2 presenting the larger bias (0.478) and PHYDRO the lowest one (0.380; Figure 2d).

Unlike for A_{net}, the models' performance for g_s in terms of Pearson's correlation, m, RMSE, and bias was generally not affected by the inclusion of acclimation (Figures S1 and S6). Acclimation led to

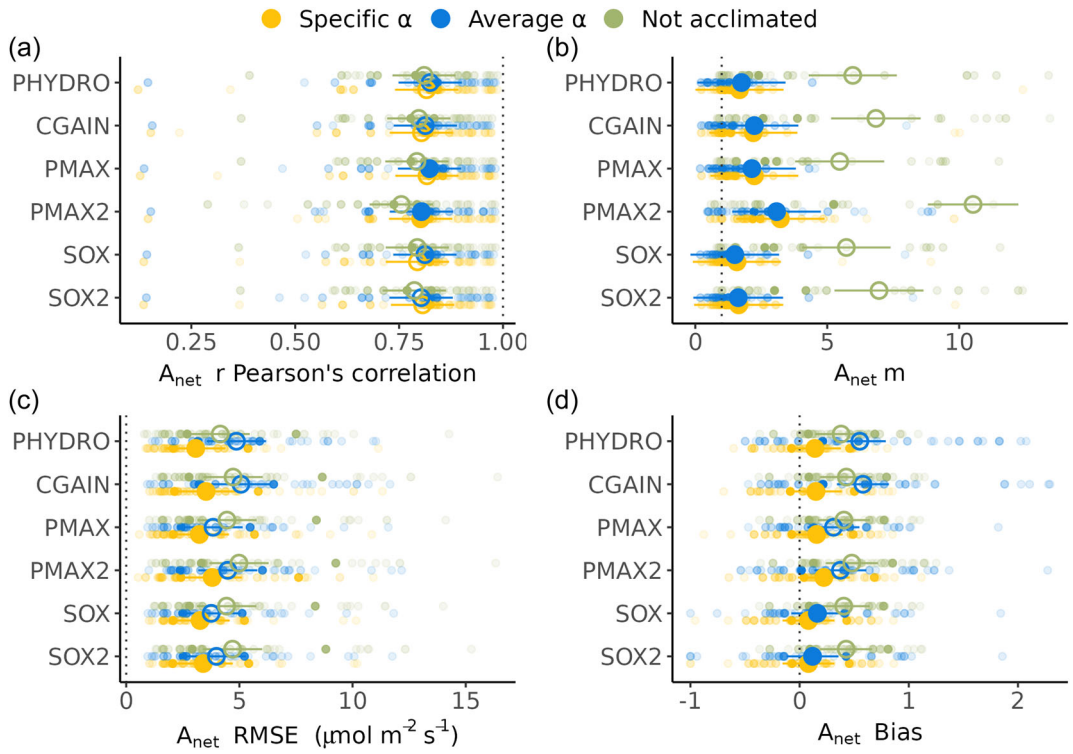

FIGURE 2 Performance comparison between acclimated and non-acclimated stomatal optimisation models, relative to species-specific observations of A_{net} during different dry-down experiments. All the performance metrics were calculated for estimates of A_{net} obtained within their full data sample, having fitted just one hydraulic parameter per stomatal model on the 80th wet percentile of the species data samples (not acclimated), then acclimating by setting α to 0.0962 for all the species (average α), and finally acclimating with a specific α. For all the models except PHYDRO we used the species-level vulnerability curve parameters ψ_{50} and b shown in Table S1. For PHYDRO, we used species-level outside-xylem vulnerability curve parameters as $\psi_{ox50} = \psi_{50}/3$ and $b = 1$. Small circles are the values for each species within each dry-down experiment, higher transparency indicates smaller data sample. Large circles are the metric averages estimated using an LMM (see Section 2). Large closed circles indicate a significant difference in the metric averages of the model realisations with acclimation with respect to not acclimated ones; conversely, large open circles indicate no significant difference between the acclimated and non-acclimation realisations. Models without acclimation are consistently represented by open circles. Statistical significance was calculated using paired t-test comparisons. Vertical dotted lines indicate the best achievable performance for each metric. (a) Pearson's correlation (b) slope (m) of the linear relationship between the actual and estimated A_{net} (c) RMSE (d) bias of the estimation of A_{net} calculated as in Equation (10). [Color figure can be viewed at wileyonlinelibrary.com]

a significant improvement of proportionality for CGAIN and PMAX2 (Figure S6b). However, m was still significantly higher than 1 for PMAX2, pointing to these models' failure to produce estimates of g_s in good proportionality with the observations (Figure S6b).

All models except PMAX were highly sensitive to the parameterisation of the species-specific vulnerability curves (Figure S7). Indeed, poor predictions resulted when parameters other than those prescribed in the respective model designs were used. Using outside-xylem vulnerability curve (ox) parameters, both SOX and SOX2 showed enhanced sensitivity to changes in ψ_s, leading to strong and rapid stomatal closure as the soil dried out (Figure S7b and S7d). CGAIN became unstable, and for several species, the model failed to converge. By contrast, PMAX2 showed improved performance (Figure S7) and, thus, similar estimates to PMAX. Likewise, using standard xylem-based vulnerability curve parameters, PHYDRO was unable to accurately depict the decline of A_{net} as the soil dried out (Figure S7b).

3.2 | Hydraulic impairment versus limitations due to photosynthetic acclimation

The proportion of variance in A_{net} explained by hydraulic (stomatal limitation) and metabolic impairment (photosynthetic acclimation limitation to photosynthesis) differed among models (Figure 3). Overall, stomatal limitations were markedly more important than metabolic impairment for all models across all conditions (Figure 3a), except for PMAX2 for which stomatal limitation and metabolic impairment were about equally important. When analysing the drier half of the data, the variance explained by photosynthetic acclimation limitations slightly decreased for all models (Figure 3b). The acclimated PHYDRO model explained the greatest variability in A_{net}, with a marginal R^2 of 0.627 for all data points (stomatal + photosynthetic acclimation contributions), whereas the acclimated PMAX and PMAX2 were the best models for the drier half of the data, achieving a marginal R^2 of 0.555 and 0.564, respectively. The proportion of variance explained by species identity was

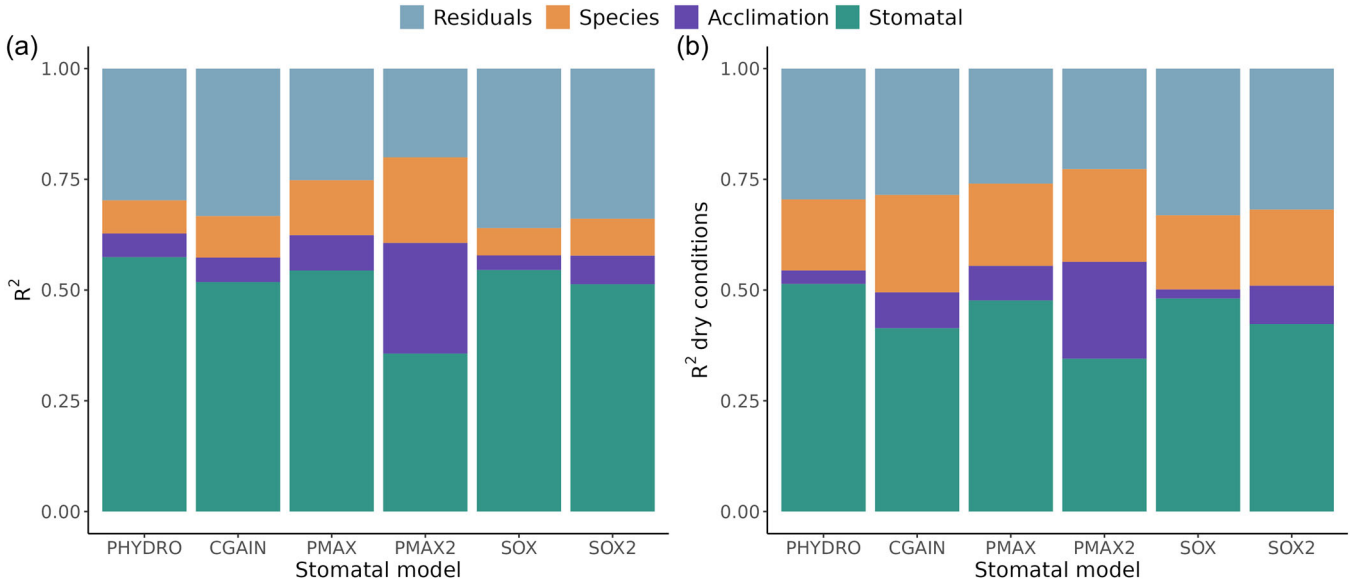

FIGURE 3 Fractions of variance in A_{net} explained by stomatal, photosynthetic acclimation, and species-level contributions for each model. (a) Partition using all the data (b) partition using the drier 50th percentile data for each species. Grey portions represent any residual variance not explained by stomatal, photosynthetic acclimation, or species contributions. [Color figure can be viewed at wileyonlinelibrary.com]

greater for the drier half of the data (Figure 3a), accounting for nearly half of the variance explained by the stomatal and photosynthetic acclimation components taken together and indicating that drier conditions elicit a greater diversity of responses among species.

3.3 | Relationship between α, functional traits, and the growth environment

Calibrating {K_{max}, ψ_{50}, b, α} for each model, species, and data source (and additionally, γ, δ or ϖ, for PHYDRO, SOX2, and CGAIN, respectively) (Calibration 3) enabled a majority of the models to match or exceed a R^2 of 0.6 for both g_s and A_{net} (Table S4); PMAX2 was an exception failing to exceed 0.6 for g_s. The combination of these R^2 values and the narrow confidence interval for the average α (0.09613–0.09689), gave us confidence in the average α obtained both across and within models. The PHYDRO and CGAIN models, which require an additional hydraulic cost parameter, exhibited a significantly higher average α (>0.1035) than other models, all of which yielded average α values significantly different from one another (α between 0.0901 and 0.0935; Figure 4). Despite these differences, none of the model's average α was different from the average α across models (α = 0.0962) nor different from 0.1, the value proposed by Joshi et al., 2022 for global applications.

A multivariate LMM combined with a stepwise AIC variable selection (Table 1) revealed three plant traits and growing conditions to explain a moderate part of the variability in α across species (marginal R^2 = 0.47), out of the eight potential explanatory variables originally considered. The species maximum height and $J_{maxWW,25}$ (i.e., the $J_{max,25}$ inferred from observations

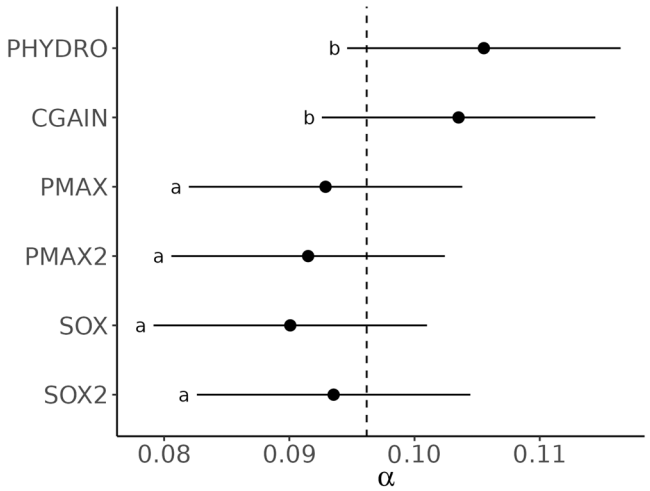

FIGURE 4 Average model-specific estimate of α across species, accounting for the random effects of the species and dry-down experiments. Vertical dashed line show the average α across models (α = 0.0962). Letters represent groups with significant differences calculated using Sidak's multiple comparison test.

under well-watered conditions) were negatively related to α, whilst the average I_{abs} had a positive relationship with α (Table 1 and Figure 5). Multicollinearity was low across the explanatory variables (VIF; Table 1). The results were similar albeit explaining a larger part of the variability (R^2 = 0.55) when the relationships between $\alpha J_{maxWW,25}$ and the eight potential explanatory variables were explored (Figure S8). In that latter case, six explanatory variables were selected: the *SLA* and maximum height of the species were associated with lower photosynthetic capacity cost under well-watered conditions, whilst I_{abs}, species K_L, *Hv*, and ψ_{50} were positively related to $\alpha J_{maxWW,25}$ (Figure S8).

4 | DISCUSSION

We have shown that including a maintenance cost for photosynthetic capacity, as proposed by Joshi et al. (2022), improves A_{net} predictions (Figure 2) across a range of hydraulics-enabled stomatal optimality frameworks, particularly under drought (Figure 2b). Our approach eliminates the need for species-level knowledge of photosynthetic capacity ($J_{max,25}$ and $V_{cmax,25}$), and for empirical functions describing the slow acclimation of photosynthetic capacity to drought (Drake, 2017; Egea et al., 2011; Keenan et al., 2009; Knauer et al., 2019; Yang et al., 2019; Zhou et al., 2013, 2014) or semi-empirical functions relating photosynthetic capacity to leaf nitrogen (Sabot et al., 2022a). Despite these benefits, our approach requires fitting an additional photosynthetic cost parameter α, whose variable responses to species-specific traits and environmental conditions remain unclear. Nonetheless, our results suggest that the cost parameter α could be predicted from plant functional traits and growth conditions.

Despite variability in model-specific α values (Figure 4), our analysis revealed a strong relationship between α and $J_{maxWW,25}$, implying that plants with higher photosynthetic capacity tend to have lower relative photosynthetic costs under well-watered conditions. Interestingly, we found a positive relationship between α and I_{abs} which suggests that species experiencing higher light intensities have higher leaf maintenance costs per unit $J_{max,25}$. This result is consistent with experimentally observed lower respiration rates in shade-tolerant plants (Reich, 2014). There is also evidence of more pronounced photo-inhibition for leaves under high light intensities exposed to moderate to severe water deficits, compared to leaves under low radiation (Epron & Dreyer, 1990; Kaiser, 1987). This suggests an enhanced photosynthetic sensitivity to drought (i.e., a higher α) for high $J_{max,25}$ leaves, perhaps linked to the production costs of photoprotective compounds whose concentrations acclimate to UV radiation levels (Barnes et al., 2023). Further, considering the strong positive correlation between I_{abs} and VPD and air temperature (Figure S3), it is likely that the increased cost associated with elevated radiation is influenced by the confounding effect of higher atmospheric aridity. Besides its relations to environmental drivers, α was negatively related to species maximum height and the total cost $\alpha J_{maxWW,25}$ was positively related to ψ_{50} and K_L (Figure S8). This suggests a potential link between the photosynthetic cost and the hydraulic safety-efficiency trade-off. However, note that all woody plants included in this study were seedlings, and many of them were far from their maximum potential heights.

Note that $\alpha J_{max,25}$ represents 60%–80% of carbon assimilation under well-watered conditions (Figure S9), while leaf respiration typically represents only about 1.5% (Collatz et al., 1991). Therefore, $\alpha J_{max,25}$ does not merely refer to leaf respiration. $\alpha J_{max,25}$ could

TABLE 1 Multivariate linear-mixed effects model (LMM) best explaining the variability of α for the fully calibrated stomatal optimisation models (Calibration 3).

	Estimate	SE	VIF	*T*-value	*p*-value
Intercept	2.01×10^{-1}	1.07×10^{-2}		18.85	<0.001
I_{abs}	6.06×10^{-5}	3.52×10^{-6}	1.04	17.24	<0.001
$J_{maxWW,25}$	-3.19×10^{-2}	2.03×10^{-3}	1.49	−15.76	<0.001
H_{max}	-8.16×10^{-3}	1.09×10^{-3}	1.48	−7.52	<0.001

Note: I_{abs} is the average absorbed photosynthetically active photon flux density during the experiment in μmol m^{-2} s^{-1}. $J_{maxWW,25}$ is the maximum electron transport capacity at standard temperature (25°C) inferred from observations under well-watered conditions, in loge ($J_{maxWW,25}$/μmolc m^{-2} s^{-1}). H_{max} is the species maximum height in m. The estimate, SE, and VIF columns stand for the estimated coefficients, standard error, and variance inflation factor.

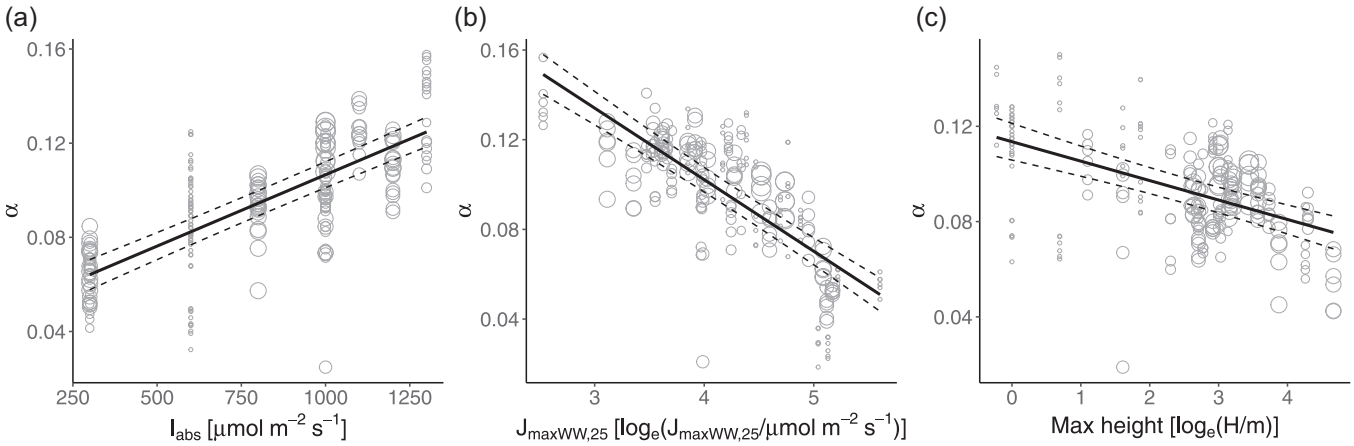

FIGURE 5 Partial effects from a multivariate linear-mixed model (LMM) explaining the variability of α. The LMM was fitted using the dry-down experiments and stomatal models as crossed random intercepts and the LMM coefficients are shown in Table 1. Grey scatter open points show all the model-specific contributions to α, across all species. Black plain lines are partial regressions and dashed lines represent the partial regressions plus or minus their standard error. Size of the points represent the weight applied to each data point, which is equal to the natural logarithm of the sample size (Table S1).

additionally encompass the carbon costs associated with maintaining the efficiency and activity of chlorophyll, the rate of RuBP regeneration, and potentially the costs of nitrogen acquisition, including allocations to fine roots, mycorrhizae, and the rhizosphere. Moreover, were $\alpha J_{max,25}$ encompassing the real carbon costs arising from respiration, it would include the respiration of all supporting organs (such as stem and roots) relative to the given leaf area. Alternatively, $\alpha J_{max,25}$ and hydraulic costs could be viewed as apparent fitness costs, linked to future mortality risks and caused by either overly risky hydraulic behaviour or excessive investment in J_{max} at the expense of other functions. In summary, the exact meaning of the parameter α remains undetermined.

Our approach diverges from the original work of Joshi et al. (2022), as we employ $\alpha J_{max,25}$ instead of αJ_{max} within our optimality criterion. This raises the question of what plants are actually acclimating to. Using $J_{max,25}$ should reflect the actual tissue-level carbon investment, as the temperature effects on photosynthetic capacity are corrected. This, in turn facilitates the comparative analyses between experiments conducted under varying growth temperatures. Another perspective suggest that plants may prioritise metabolic costs, which are temperature-dependent, over tissue investment, thus optimising the realised J_{max}. Temperature significantly influences $J_{max,25}$ which decreases as growth temperature increases (Crous et al., 2022; Fürstenau Togashi et al., 2018). This suggests that the cost term could be αJ_{max} as proposed in Joshi et al. (2022). However, an increase in temperature also decreases the ratio of $J_{max,25}$ to $V_{cmax,25}$, albeit at a different pace than it does $J_{max,25}$ alone (Crous et al., 2022). This suggests that α might need its own temperature response function to accommodate the varying rates of change, thus requiring a temperature-normalised α and allowing the use of $J_{max,25}$. Whether the photosynthetic costs parameter α changes through time or increases during dry-downs is not resolved by our analysis, but the magnitude of α might also depend on hydraulic impairment. Given these considerations, the choice of the cost term (i.e., $\alpha J_{max,25}$ or αJ_{max}) warrants further investigation.

With the caveat that performance evaluation of the models presented here only accounts for model predictions of A_{net} and g_s, PMAX performed best when photosynthetic acclimation was included (Figures 2 and 3). Previous studies have shown this stomatal optimisation model to perform as well or better than empirical stomatal models in the absence of photosynthetic acclimation (Sabot et al., 2020; Sabot et al., 2022b; Venturas et al., 2018; Wang et al., 2020), and it has also been shown to make robust predictions when accounting for it (Sabot et al., 2022a). The SOX, SOX2, PHYDRO, and CGAIN also showed reasonably good performance (Figures 2 and 3), especially in terms of improvement to proportionality when acclimation was considered (Figure 2b), but note that these four models were more sensitive to the choice of vulnerability curve parameters than PMAX (cf. Figure 2 and Figure S7). In stark contrast, even though the inclusion of photosynthetic acclimation improved the performance of PMAX2 in terms of correlation, RMSE, and bias, it did not improve the proportionality of their A_{net} predictions (Figure 2b), except when outside-xylem vulnerability curve (ox) parameters were used (Figure S7). Overall, and in line with the findings of Sabot et al. (2022b), our simulations' performance without acclimation did not support the assertion by Wang et al. (2020) that PMAX2 (neither a variation of PMAX2; see Notes 2 in the Supporting Information Material) outperforms other stomatal optimisation models. Compared to other existing models that relate non-stomatal limitations to hydraulic function (e.g., Novick et al., 2016; Dewar et al., 2018; Dewar et al., 2021; Hölttä et al., 2017; Nadal-Sala et al., 2021; Yang et al., 2019), the acclimated models presented in this study (and Joshi et al., 2022) solely account for changes in photosynthetic capacity. Consequently, our models assume a less conservative stomatal behaviour because they do not account for the full feedback effect of a change in ψ_l on V_{cmax} and J_{max} and of a marginal change in V_{cmax} and J_{max} on the optimal behaviour.

Stomatal optimisation models, particularly when incorporating photosynthetic acclimation and calibrated hydraulic parameters, exhibit sufficient flexibility to reasonably predict A_{net} and g_s under varying soil moisture conditions, which is essential in forecasting global carbon and water cycles. Although effective for several species and models, the time-intensive optimisation required by large parameter calibrations (e.g., Calibration 3) limits its feasibility for large-scale databases. This limitation can be addressed by using hydraulic parameters at the species or ecosystem level, thus reducing the number of parameters requiring calibration (e.g., Calibration 1). However, these models might not perform so well when directly parameterised based on both hydraulic vulnerability curves and estimates of K_{max} for a given plant organ (e.g., leaf, branch, stem, root), especially if taken in isolation from photosynthetic acclimation parameters. This is important as it is still not fully understood how the scaling of organ-level vulnerability curves represents the entire hydraulic system (Wang and Frankenberg, 2022b) and how all traits coordinate at the plant level (McCulloh et al., 2019). Nonetheless, ongoing research is advancing our knowledge of global plant traits and their coordination (Sanchez-Martinez et al., 2023; Xu et al., 2021), presenting opportunities for improved and generalised utilisation of stomatal optimisation models.

ACKNOWLEDGEMENTS

The authors would like to express their gratitude to all the contributors to the research from which the experimental data were drawn, and especially Jaume Flexas and Jeroni Galmes for sharing their original database. Additionally, the authors extend their thanks to Shuangxi Zhou, who compiled the first version of the database used in this study, to Rafael Poyatos for providing access to computing facilities, and to Rodolfo Nóbrega for the key discussions at an early stage of the study. We would like to thank Stefano Manzoni and one anonymous reviewer for their constructive suggestions. Victor Flo acknowledges support from the Margarita Salas grant (698511) funded by MICIU/AEI/10.13039/501100011033 and by European Union NextGenerationEU/PRTR. Manon Sabot acknowledges support from the Australian Research Council (ARC) Centre of Excellence for Climate Extremes (CE170100023), as well as an ARC Discovery Grant (DP190101823).

Jaideep Joshi gratefully acknowledges funding from the European Union's Horizon 2020 research and innovation programme under the Marie Skłodowska-Curie Actions fellowship (Grant Agreement No. 841283 – Plant-FATE), the Strategic Initiatives Program of the International Institute for Applied Systems Analysis (IIASA; Project name – RESIST), and the National Member Organizations that support IIASA. David Sandoval and Colin Prentice acknowledge support from the funding from the LEMONTREE (Land Ecosystem Models based On New Theory, obseRvations and ExperimEnts) project, funded through the generosity of Eric and Wendy Schmidt by reccommendaton of the Schmidt Futures programme. Colin Prentice also acknowledges funding from the European Research Council (ERC) under the European Union's Horizon 2020 research and innovation programme (Grant Agreement No. 787203 REALM).

DATA AVAILABILITY STATEMENT

The data that support the findings of this study are openly available in Acclimated_gs_optimization_models at https://github.com/vflo/Acclimated_gs_optimization_models.

ORCID

Victor Flo https://orcid.org/0000-0003-1908-4577
Jaideep Joshi https://orcid.org/0000-0003-1315-6234
Manon Sabot https://orcid.org/0000-0002-9440-4553
David Sandoval https://orcid.org/0000-0002-4404-6452
Iain Colin Prentice https://orcid.org/0000-0002-1296-6764

REFERENCES

Ahlström, A., Raupach, M.R., Schurgers, G., Smith, B., Arneth, A. & Jung, M. et al. (2015) The dominant role of semi-arid ecosystems in the trend and variability of the land CO_2 sink. *Science*, 348(6237), 895–899. Available from: https://doi.org/10.1126/science.aaa1668

Anderegg, W.R.L., Wolf, A., Arango-Velez, A., Choat, B., Chmura, D.J., Jansen, S. et al. (2018) Woody plants optimise stomatal behaviour relative to hydraulic risk. D. Cameron (ed.) *Ecology Letters*, 21(7), 968–977. Available from: https://doi.org/10.1111/ele.12962

Arora, V.K., Katavouta, A., Williams, R.G., Jones, C.D., Brovkin, V. et al. (2020) Carbon–concentration and carbon–climate feedbacks in CMIP6 models and their comparison to CMIP5 models. *Biogeosciences*, 17(16), 4173–4222. Available from: https://doi.org/10.5194/bg-17-4173-2020

Ball, J.T., Woodrow, I.E. & Berry, J.A. (1987) A Model Predicting Stomatal Conductance and its Contribution to the Control of Photosynthesis under Different Environmental Conditions. In: Biggins, J. (ed.). *Progress in Photosynthesis Research: Volume 4 Proceedings of the VIIth International Congress on Photosynthesis Providence, Rhode Island, USA, August 10–15, 1986*. Dordrecht, Springer Netherlands. p. 221–224. https://doi.org/10.1007/978-94-017-0519-6_48

Barnes, P.W., Robson, T.M., Zepp, R.G., Bornman, J.F., Jansen, M.A.K., Ossola, R. et al. (2023) Interactive effects of changes in UV radiation and climate on terrestrial ecosystems, biogeochemical cycles, and feedbacks to the climate system. *Photochemical & Photobiological Sciences*, 22, 1049–1091. Available from: https://doi.org/10.1007/s43630-023-00376-7

Bartoń, K. (2020) MuMIn: multi-model inference. *R package version 1.43.17*. https://CRAN.R-project.org/package=MuMIn

Bates, D., Mächler, M., Bolker, B. & Walker, S. (2015) Fitting linear mixed-effects models using lme4. *Journal of Statistical Software*, 67(1), 1–48. Available from: https://doi.org/10.18637/jss.v067.i01

Buckley, T.N., Frehner, E.H. & Bailey, B.N. (2023) Kinetic factors of physiology and the dynamic light environment influence the economic landscape of short-term hydraulic risk. *New Phytologist*, 238, 529–548. Available from: https://doi.org/10.1111/nph.18739

Caldararu, S., Thum, T., Yu, L. & Zaehle, S. (2020) Whole-plant optimality predicts changes in leaf nitrogen under variable CO_2 and nutrient availability. *New Phytologist*, 225(6), 2331–2346. Available from: https://doi.org/10.1111/nph.16327

Chen, J.-L., Reynolds, J.F., Harley, P.C. & Tenhunen, J.D. (1993) Coordination theory of leaf nitrogen distribution in a canopy. *Oecologia*, 93(1), 63–69. Available from: https://doi.org/10.1007/BF00321192

Choat, B., Jansen, S., Brodribb, T.J., Cochard, H., Delzon, S. & Bhaskar, R. et al. (2012) Global convergence in the vulnerability of forests to drought. *Nature*, 491(7426), 752–755. Available from: https://doi.org/10.1038/nature11688

Collatz, G.J., Ball, J.T., Grivet, C. & Berry, J.A. (1991) Physiological and environmental regulation of stomatal conductance, photosynthesis and transpiration: a model that includes a laminar boundary layer. *Agricultural and Forest Meteorology*, 54, 107–136.

Cowan, I.R. & Farquhar, G.D. (1977) Stomatal function in relation to leaf metabolism and environment. *Symposia of the Society for Experimental Biology*, 31, 471–505.

Crous, K.Y., Uddling, J. & De Kauwe, M.G. (2022) Temperature responses of photosynthesis and respiration in evergreen trees from boreal to tropical latitudes. *New Phytologist*, 234(2), 353–374. Available from: https://doi.org/10.1111/nph.17951

Dewar, R., Hölttä, T. & Salmon, Y. (2021) Exploring optimal stomatal control under alternative hypotheses for the regulation of plant sources and sinks. *New Phytologist*, 233(2), 639–654. Available from: https://doi.org/10.1111/nph.17795

Dewar, R., Mauranen, A., Mäkelä, A., Hölttä, T., Medlyn, B. & Vesala, T. (2018) New insights into the covariation of stomatal, mesophyll and hydraulic conductances from optimization models incorporating nonstomatal limitations to photosynthesis. *New Phytologist*, 217(2), 571–585. Available from: https://doi.org/10.1111/nph.14848

Drake, J.E., Power, S.A., Duursma, R.A., Medlyn, B.E., Aspinwall, M.J., Choat, B., et al. (2017) Stomatal and non-stomatal limitations of photosynthesis for four tree species under drought: a comparison of model formulations. *Agricultural and Forest Meteorology*, 247, 454–466.

Egea, G., Verhoef, A. & Vidale, P.L. (2011) Towards an improved and more flexible representation of water stress in coupled photosynthesis–stomatal conductance models. *Agricultural and Forest Meteorology*, 151(10), 1370–1384. Available from: https://doi.org/10.1016/j.agrformet.2011.05.019

Eller, C.B., Rowland, L., Mencuccini, M., Rosas, T., Williams, K. & Choat, B. et al. (2020) Stomatal optimization based on xylem hydraulics (SOX) improves land surface model simulation of vegetation responses to climate. *New Phytologist*, 226(6), 1622–1637. Available from: https://doi.org/10.1111/nph.16419

Eller, C.B., Rowland, L., Oliveira, R.S., Bittencourt, P.R.L., Barros, F.V. & da Costa, A.C.L. et al. (2018) Modelling tropical forest responses to drought and El Niño with a stomatal optimization model based on xylem hydraulics. *Philosophical Transactions of the Royal Society B: Biological Sciences*, 373(1760), 20170315. Available from: https://doi.org/10.1098/rstb.2017.0315

Epron, D. & Dreyer, E. (1990) Stomatal and non stomatal limitation of photosynthesis by leaf water deficits in three oak species: a comparison of gas exchange and chlorophyll a fluorescence data. *Annales des Sciences Forestières*, 47(5), 435–450. Available from: https://doi.org/10.1051/forest:19900503

Farquhar, G.D., von Caemmerer, S. & Berry, J.A. (1980) A biochemical model of photosynthetic CO2 assimilation in leaves of C3 species. *Planta*, 149(1), 78–90. Available from: https://doi.org/10.1007/BF00386231

Feng, X., Lu, Y., Jiang, M., Katul, G., Manzoni, S., Mrad, A. et al. (2022) Instantaneous stomatal optimization results in suboptimal carbon gain due to legacy effects. *Plant, Cell & Environment*, 45(11), 3189–3204. Available from: https://doi.org/10.1111/pce.14427

Fisher, R.A. & Koven, C.D. (2020) Perspectives on the future of land surface models and the challenges of representing complex terrestrial systems. *Journal of Advances in Modeling Earth Systems*, 12(4), e2018MS001453. Available from: https://doi.org/10.1029/2018MS001453

Flexas, J. & Medrano, H. (2002) Drought-inhibition of photosynthesis in C3 plants: stomatal and non-stomatal limitations revisited. *Annals of Botany*, 89(2), 183–189. Available from: https://doi.org/10.1093/aob/mcf027

Friend, A.D. (1991) Use of a model of photosynthesis and leaf microenvironment to predict optimal stomatal conductance and leaf nitrogen partitioning. *Plant, Cell & Environment*, 14(9), 895–905. Available from: https://doi.org/10.1111/j.1365-3040.1991.tb00958.x

Fürstenau Togashi, H., Prentice, I.C., Atkin, O.K., Macfarlane, C., Prober, S.M., Bloomfield, K.J. et al. (2018) Thermal acclimation of leaf photosynthetic traits in an evergreen woodland, consistent with the coordination hypothesis. *Biogeosciences*, 15(11), 3461–3474. Available from: https://doi.org/10.5194/bg-15-3461-2018

Green, J.K., Seneviratne, S.I., Berg, A.M., Findell, K.L., Hagemann, S., Lawrence, D.M. et al. (2019) Large influence of soil moisture on long-term terrestrial carbon uptake. *Nature*, 565(7740), 476–479. Available from: https://doi.org/10.1038/s41586-018-0848-x

Haverd, V., Smith, B., Nieradzik, L., Briggs, P.R., Woodgate, W., Trudinger, C.M. et al. (2018) A new version of the CABLE land surface model (Subversion revision r4601) incorporating land use and land cover change, woody vegetation demography, and a novel optimisation-based approach to plant coordination of photosynthesis. *Geoscientific Model Development*, 11(7), 2995–3026. Available from: https://doi.org/10.5194/gmd-11-2995-2018

Hölttä, T., Lintunen, A., Chan, T., Mäkelä, A. & Nikinmaa, E. (2017) A steady-state stomatal model of balanced leaf gas exchange, hydraulics and maximal source–sink flux. *Tree Physiology*, 37(7), 851–868. Available from: https://doi.org/10.1093/treephys/tpx011

Humphrey, V., Berg, A., Ciais, P., Gentine, P., Jung, M., Reichstein, M. et al. (2021) Soil moisture–atmosphere feedback dominates land carbon uptake variability. *Nature*, 592(7852), 65–69. Available from: https://doi.org/10.1038/s41586-021-03325-5

Jiang, C., Ryu, Y., Wang, H. & Keenan, T.F. (2020) An optimality-based model explains seasonal variation in C3 plant photosynthetic capacity. *Global Change Biology*, 26(11), 6493–6510. Available from: https://doi.org/10.1111/gcb.15276

Joshi, J., Stocker, B.D., Hofhansl, F., Zhou, S., Dieckmann, U. & Prentice, I.C. (2022) Towards a unified theory of plant photosynthesis and hydraulics. *Nature Plants*, 8(11), 1304–1316. Available from: https://doi.org/10.1038/s41477-022-01244-5

Kaiser, W.M. (1987) Effects of water deficit on photosynthetic capacity. *Physiologia Plantarum*, 71(1), 142–149. Available from: https://doi.org/10.1111/j.1399-3054.1987.tb04631.x

Kannenberg, S.A., Schwalm, C.R. & Anderegg, W.R.L. (2020) Ghosts of the past: how drought legacy effects shape forest functioning and carbon cycling. M. Rejmanek (ed.) *Ecology Letters*, 23(5), 891–901. Available from: https://doi.org/10.1111/ele.13485

Karger, D.N., Conrad, O., Böhner, J., Kawohl, T., Kreft, H., Soria-Auza, R.W. et al. (2017) Climatologies at high resolution for the earth's land surface areas. *Scientific Data*, 4(1), 170122. Available from: https://doi.org/10.1038/sdata.2017.122

Katul, G.G., Palmroth, S. & Oren, R. (2009) Leaf stomatal responses to vapour pressure deficit under current and CO_2 -enriched atmosphere explained by the economics of gas exchange. *Plant, Cell & Environment*, 32(8), 968–979. Available from: https://doi.org/10.1111/j.1365-3040.2009.01977.x

De Kauwe, M.G., Lin, Y., Wright, I.J., Medlyn, B.E., Crous, K.Y. & Ellsworth, D. et al. (2016) A test of the 'one-point method' for estimating maximum carboxylation capacity from field-measured, light-saturated photosynthesis. *New Phytologist*, 210(3), 1130–1144. Available from: https://doi.org/10.1111/nph.13815

Keenan, T., Garcıa, R., Friend, A.D., Zaehle, S., Gracia, C. & Sabate, S. (2009) *Improved understanding of drought controls on seasonal variation in Mediterranean forest canopy CO_2 and water fluxes through combined in situ measurements and ecosystem modelling*.

Knauer, J., Zaehle, S., De Kauwe, M.G., Bahar, N.H.A., Evans, J.R., Medlyn, B.E. et al. (2019) Effects of mesophyll conductance on vegetation responses to elevated CO_2 concentrations in a land surface model. *Global Change Biology*, 25(5), 1820–1838. Available from: https://doi.org/10.1111/gcb.14604

Konrad, W., Roth-Nebelsick, A. & Grein, M. (2008) Modelling of stomatal density response to atmospheric. *Journal of Theoretical Biology*, 253(4), 638–658. Available from: https://doi.org/10.1016/j.jtbi.2008.03.032

Leuning, R. (1990) Modelling stomatal behaviour and and photosynthesis of *Eucalyptus grandis*. *Functional Plant Biology*, 17(2), 159. Available from: https://doi.org/10.1071/PP9900159

Leuning, R. (1995) A critical appraisal of a combined stomatal-photosynthesis model for C3 plants. *Plant, Cell and Environment*, 18(4), 339–355. Available from: https://doi.org/10.1111/j.1365-3040.1995.tb00370.x

Lombardozzi, D.L., Bonan, G.B., Smith, N.G., Dukes, J.S. & Fisher, R.A. (2015) Temperature acclimation of photosynthesis and respiration: a key uncertainty in the carbon cycle-climate feedback. *Geophysical Research Letters*, 42(20), 8624–8631. Available from: https://doi.org/10.1002/2015GL065934

Lu, Y., Duursma, R.A., Farrior, C.E., Medlyn, B.E. & Feng, X. (2020) Optimal stomatal drought response shaped by competition for water and hydraulic risk can explain plant trait covariation. *New Phytologist*, 225(3), 1206–1217. Available from: https://doi.org/10.1111/nph.16207

Maire, V., Martre, P., Kattge, J., Gastal, F., Esser, G., Fontaine, S. et al. (2012) The coordination of leaf photosynthesis links C and N fluxes in C3 plant species. B. Bond-Lamberty (ed.) *PLoS One*, 7(6), e38345. Available from: https://doi.org/10.1371/journal.pone.0038345

Mäkelä, A. (1996) Optimal control of gas exchange during drought: theoretical analysis. *Annals of Botany*, 77(5), 461–468. Available from: https://doi.org/10.1006/anbo.1996.0056

Manzoni, S., Vico, G., Katul, G., Fay, P.A., Polley, W., Palmroth, S. et al. (2011) Optimizing stomatal conductance for maximum carbon gain under water stress: a meta-analysis across plant functional types and climates. *Functional Ecology*, 25(3), 456–467. Available from: https://doi.org/10.1111/j.1365-2435.2010.01822.x

Manzoni, S., Vico, G., Palmroth, S., Porporato, A. & Katul, G. (2013) Optimization of stomatal conductance for maximum carbon gain under dynamic soil moisture. *Advances in Water Resources*, 62(PA), 90–105. Available from: https://doi.org/10.1016/j.advwatres.2013.09.020

Martin-StPaul, N., Delzon, S. & Cochard, H. (2017) Plant resistance to drought depends on timely stomatal closure. H. Maherali (ed.) *Ecology Letters*, 20(11), 1437–1447. Available from: https://doi.org/10.1111/ele.12851

Martin-StPaul, N.K., Limousin, J.-M., Rodríguez-Calcerrada, J., Ruffault, J., Rambal, S., Letts, M.G. et al. (2012) Photosynthetic sensitivity to drought varies among populations of *Quercus ilex* along a rainfall

gradient. *Functional Plant Biology*, 39(1), 25. Available from: https://doi.org/10.1071/FP11090

McCulloh, K.A., Domec, J., Johnson, D.M., Smith, D.D. & Meinzer, F.C. (2019) A dynamic yet vulnerable pipeline: integration and coordination of hydraulic traits across whole plants. *Plant, Cell & Environment*, 42(10), 2789–2807. Available from: https://doi.org/10.1111/pce.13607

Medlyn, B.E., Duursma, R.A., Eamus, D., Ellsworth, D.S., Prentice, I.C., Barton, C.V.M. et al. (2011) Reconciling the optimal and empirical approaches to modelling stomatal conductance: reconciling optimal and empirical stomatal models. *Global Change Biology*, 17(6), 2134–2144. Available from: https://doi.org/10.1111/j.1365-2486.2010.02375.x

Mencuccini, M., Manzoni, S. & Christoffersen, B. (2019) Modelling water fluxes in plants: from tissues to biosphere. *New Phytologist*, 222(3), 1207–1222. Available from: https://doi.org/10.1111/nph.15681

Mercado, L.M., Medlyn, B.E., Huntingford, C., Oliver, R.J., Clark, D.B., Sitch, S. et al. (2018) Large sensitivity in land carbon storage due to geographical and temporal variation in the thermal response of photosynthetic capacity. *New Phytologist*, 218(4), 1462–1477. Available from: https://doi.org/10.1111/nph.15100

Mullen, K., Ardia, D., Gil, D., Windover, D. & Cline, J. (2011) DEoptim: an *R* package for global optimization by differential evolution. *Journal of Statistical Software*, 40(6), 1–26. Available from: https://doi.org/10.18637/jss.v040.i06

Nadal-Sala, D., Grote, R., Birami, B., Knüver, T., Rehschuh, R., & Schwarz, S. et al. (2021) Leaf shedding and non-stomatal limitations of photosynthesis mitigate hydraulic conductance losses in scots pine saplings during severe drought stress. *Frontiers in Plant Science*, 12. Available from: https://doi.org/10.3389/fpls.2021.715127

Novick, K.A., Miniat, C.F. & Vose, J.M. (2016) Drought limitations to leaf-level gas exchange: Results from a model linking stomatal optimization and cohesion–tension theory. *Plant, Cell & Environment*, 39(3), 583–596. Available from: https://doi.org/10.1111/pce.12657

Peguero-Pina, J.J., Sancho-Knapik, D., Morales, F., Flexas, J. & Gil-Pelegrín, E. (2009) Differential photosynthetic performance and photoprotection mechanisms of three Mediterranean evergreen oaks under severe drought stress. *Functional Plant Biology*, 36(5), 453. Available from: https://doi.org/10.1071/FP08297

Prentice, I.C., Liang, X., Medlyn, B.E. & Wang, Y.-P. (2015) Reliable, robust and realistic: the three R's of next-generation land-surface modelling. *Atmospheric Chemistry and Physics*, 15(10), 5987–6005. Available from: https://doi.org/10.5194/acp-15-5987-2015

R Core Team (2022) *R: A Language and Environment for Statistical Computing*. https://www.R-project.org/

Reich, P.B. (2014) The world-wide 'fast-slow' plant economics spectrum: a traits manifesto. *Journal of Ecology*, 102(2), 275–301. Available from: https://doi.org/10.1111/1365-2745.12211

Rogers, A., Medlyn, B.E., Dukes, J.S., Bonan, G., Caemmerer, S., Dietze, M.C. et al. (2017) A roadmap for improving the representation of photosynthesis in earth system models. *New Phytologist*, 213(1), 22–42. Available from: https://doi.org/10.1111/nph.14283

Ruehr, N.K., Grote, R., Mayr, S. & Arneth, A. (2019) Beyond the extreme: recovery of carbon and water relations in woody plants following heat and drought stress. *Tree Physiology*, 39(8), 1285–1299. Available from: https://doi.org/10.1093/treephys/tpz032

Sabot, M.E.B., De Kauwe, M.G., Pitman, A.J., Ellsworth, D.S., Medlyn, B.E., Caldararu, S. et al. (2022a) Predicting resilience through the lens of competing adjustments to vegetation function. *Plant, Cell & Environment*, 45(9), 2744–2761. Available from: https://doi.org/10.1111/pce.14376

Sabot, M.E.B., De Kauwe, M.G., Pitman, A.J., Medlyn, B.E., Ellsworth, D.S., Martin-StPaul, N.K. et al. (2022b) One stomatal model to rule them all? Toward improved representation of carbon and water exchange in global models. *Journal of Advances in Modeling Earth Systems*, 14(4), e2021MS003761. Available from: https://doi.org/10.1029/2021MS002761

Sabot, M.E.B., De Kauwe, M.G., Pitman, A.J., Medlyn, B.E., Verhoef, A., Ukkola, A.M. et al. (2020) Plant profit maximization improves predictions of European forest responses to drought. *New Phytologist*, 226(6), 1638–1655. Available from: https://doi.org/10.1111/nph.16376

Salmon, Y., Lintunen, A., Dayet, A., Chan, T., Dewar, R., Vesala, T. et al. (2020) Leaf carbon and water status control stomatal and nonstomatal limitations of photosynthesis in trees. *New Phytologist*, 226(3), 690–703. Available from: https://doi.org/10.1111/nph.16436

Sanchez-Martinez, P., Mencuccini, M., García-Valdés, R., Hammond, W.M., Serra-Diaz, J.M., Guo, W.-Y. et al. (2023) Increased hydraulic risk in assemblages of woody plant species predicts spatial patterns of drought-induced mortality. *Nature Ecology & Evolution*, 7, 1620–1632. Available from: https://doi.org/10.1038/s41559-023-02180-z

Schymanski, S.J., Roderick, M.L., Sivapalan, M., Hutley, L.B. & Beringer, J. (2007) A canopy-scale test of the optimal water-use hypothesis. *Plant, Cell & Environment*, 31(1), 97–111. Available from: https://doi.org/10.1111/j.1365-3040.2007.01740.x

Seiler, C., Melton, J.R., Arora, V.K., Sitch, S., Friedlingstein, P., Anthoni, P. et al. (2022) Are terrestrial biosphere models fit for simulating the global land carbon sink? *Journal of Advances in Modeling Earth Systems*, 14(5). Available from: https://doi.org/10.1029/2021MS002946

Smith, N.G. & Keenan, T.F. (2020) Mechanisms underlying leaf photosynthetic acclimation to warming and elevated CO_2 as inferred from least-cost optimality theory. *Global Change Biology*, 26(9), 5202–5216. Available from: https://doi.org/10.1111/gcb.15212

Smith, N.G., Keenan, T.F., Colin Prentice, I., Wang, H., Wright, I.J. & Niinemets, U. et al. (2019) Global photosynthetic capacity is optimized to the environment. *Ecology Letters*, 22(3), 506–517. Available from: https://doi.org/10.1111/ele.13210

Sperry, J.S., Venturas, M.D., Anderegg, W.R.L., Mencuccini, M., Mackay, D.S., Wang, Y. et al. (2017) Predicting stomatal responses to the environment from the optimization of photosynthetic gain and hydraulic cost: a stomatal optimization model. *Plant, Cell & Environment*, 40(6), 816–830. Available from: https://doi.org/10.1111/pce.12852

Stocker, B.D., Zscheischler, J., Keenan, T.F., Prentice, I.C., Seneviratne, S.I. & Peñuelas, J. (2019) Drought impacts on terrestrial primary production underestimated by satellite monitoring. *Nature Geoscience*, 12(4), 264–270. Available from: https://doi.org/10.1038/s41561-019-0318-6

Sun, Y., Gu, L., Dickinson, R.E., Pallardy, S.G., Baker, J., Cao, Y. et al. (2014) Asymmetrical effects of mesophyll conductance on fundamental photosynthetic parameters and their relationships estimated from leaf gas exchange measurements: asymmetrical mesophyll conductance effects. *Plant, Cell & Environment*, 37(4), 978–994. Available from: https://doi.org/10.1111/pce.12213

Venturas, M.D., Sperry, J.S., Love, D.M., Frehner, E.H., Allred, M.G., Wang, Y. et al. (2018) A stomatal control model based on optimization of carbon gain versus hydraulic risk predicts aspen sapling responses to drought. *New Phytologist*, 220(3), 836–850. Available from: https://doi.org/10.1111/nph.15333

Wang, Y. & Frankenberg, C. (2022a) On the impact of canopy model complexity on simulated carbon, water, and solar-induced chlorophyll fluorescence fluxes. *Biogeosciences*, 19(1), 29–45. Available from: https://doi.org/10.5194/bg-19-29-2022

Wang, Y. & Frankenberg, C. (2022b) Technical note: common ambiguities in plant hydraulics. *Biogeosciences*, 19(19), 4705–4714. Available from: https://doi.org/10.5194/bg-19-4705-2022

Wang, H., Prentice, I.C., Keenan, T.F., Davis, T.W., Wright, I.J., & Cornwell, W.K., et al. (2017). Towards a universal model for carbon

dioxide uptake by plants. *Nature Plants*, 3(9), 734–741. https://doi.org/10.1038/s41477-017-0006-8

Wang, Y., Sperry, J.S., Anderegg, W.R.L., Venturas, M.D. & Trugman, A.T. (2020) A theoretical and empirical assessment of stomatal optimization modeling. *New Phytologist*, 227(2), 311–325. Available from: https://doi.org/10.1111/nph.16572

Wolf, A., Anderegg, W.R.L. & Pacala, S.W. (2016) Optimal stomatal behavior with competition for water and risk of hydraulic impairment. *Proceedings of the National Academy of Sciences*, 113(46), E7222–E7230. Available from: https://doi.org/10.1073/pnas.1615144113

Wong, S.-C., Cowan, I.R. & Farquhar, G.D. (1985) Leaf conductance in relation to rate of CO_2 assimilation: III. Influences of water stress and photoinhibition. *Plant Physiology*, 78(4), 830–834. Available from: https://doi.org/10.1104/pp.78.4.830

Xu, H., Wang, H., Prentice, I.C., Harrison, S.P. & Wright, I.J. (2021) Coordination of plant hydraulic and photosynthetic traits: confronting optimality theory with field measurements. *New Phytologist*, 232(3), 1286–1296. Available from: https://doi.org/10.1111/nph.17656

Yang, J., Duursma, R.A., De Kauwe, M.G., Kumarathunge, D., Jiang, M., Mahmud, K. et al. (2019) Incorporating non-stomatal limitation improves the performance of leaf and canopy models at high vapour pressure deficit. *Tree Physiology*, 39(12), 1961–1974. Available from: https://doi.org/10.1093/treephys/tpz103

Zhou, S., Duursma, R.A., Medlyn, B.E., Kelly, J.W.G. & Prentice, I.C. (2013) How should we model plant responses to drought? An analysis of stomatal and non-stomatal responses to water stress. *Agricultural and Forest Meteorology*, 182–183, 204–214. Available from: https://doi.org/10.1016/j.agrformet.2013.05.009

Zhou, S., Medlyn, B., Sabaté, S., Sperlich, D., Prentice, I.C. & Whitehead, D. (2014) Short-term water stress impacts on stomatal, mesophyll and biochemical limitations to photosynthesis differ consistently among tree species from contrasting climates. *Tree Physiology*, 34(10), 1035–1046. Available from: https://doi.org/10.1093/treephys/tpu072

SUPPORTING INFORMATION

Additional supporting information can be found online in the Supporting Information section at the end of this article.

How to cite this article: Flo, V., Joshi, J., Sabot, M., Sandoval, D. & Prentice, I. C. (2024) Incorporating photosynthetic acclimation improves stomatal optimisation models. *Plant, Cell & Environment*, 1–16. https://doi.org/10.1111/pce.14891